EPJ manuscript No.
(will be inserted by the editor)

Polarization Correlations in Electron–Nucleus Bremsstrahlung: The Short–Wavelength Limit

D. H. Jakubassa–Amundsen[1] and A. Surzhykov[2,3]

[1] Mathematics Institute, University of Munich, Theresienstrasse 39, 80333 Munich, Germany
[2] Physics Institute, University of Heidelberg, Philosophenweg 12, 69126 Heidelberg, Germany
[3] GSI Helmholtzzentrum für Schwerionenforschung, Planckstrasse 1, 64291 Darmstadt, Germany

the date of receipt and acceptance should be inserted later

Abstract. The short–wavelength limit of the electron–nucleus bremsstrahlung is re–investigated with special emphasis on the polarization correlations between incoming electron and emitted photons. A theoretical analysis of these correlations is performed within both the rigorous relativistic Dirac theory and the Dirac–Sommerfeld–Maue (DSM) approach which approximates the initial electronic state by a Sommerfeld–Maue wavefunction. Based on detailed calculations carried out for bremsstrahlung of electrons scattered from medium– and high–Z bare ions, we argue that the DSM approach is complementary to the exact partial–wave theory at sufficiently high collision energies. For such high–relativistic domains predictions are made for the polarization correlations relating to linearly polarized radiation.

PACS. 34.80.-i Electron and positron scattering – 41.60.-m Radiation by moving charges – 34.80.Pa Coherence and correlation

1 Introduction

The last few years have witnessed a significant progress in the development of novel–type Ge and Si(Li) Compton polarimeters [1–3]. By exploiting the polarization sensitivity of the Compton effect described by the Klein–Nishina formula [5], these solid–state detectors allow accurate measurements of the *linear* polarization of x–ray photons with energies ranging from 100 keV to a few MeV. In this energy region, Compton scattering dominates the other processes of photon–matter interaction, which are the photoelectric effect and the pair production.

When applied to the analysis of the photon emission in processes involving highly–charged, heavy ions, such polarization detectors allow to gain more insight into the structure and dynamics of heavy atomic systems. Relativistic, quantum electrodynamics (QED), and even parity–violation (PV) phenomena, which are usually difficult to isolate when studying total cross sections, often become "visible" in polarization–sensitive studies. Recently a number of experiments has been initiated to analyze polarization properties of x–rays following relativistic ion–atom and ion–electron collisions. At the GSI storage ring in Darmstadt, for example, the linear polarization of photons emitted during (and following) radiative electron capture (REC) of loosely bound target electrons by high–Z projectile ions has been studied in detail [1,6]. These studies have revealed important information about the electron–photon and electron–electron interactions in the presence of extremely strong electromagnetic fields.

Apart from (polarization) studies of free–bound electron transitions, interest has been revived in the radiative scattering of electrons by heavy target atoms and ions, i.e. the bremsstrahlung process. During the last two years, a series of polarization–resolved bremsstrahlung measurements has been carried out at the Technical University of Darmstadt. In these measurements, particular attention was paid to the investigation of how the photon polarization is affected when the incident electrons are themselves spin polarized. Such a *polarization transfer* has been observed for collisions of 100 keV electrons with a gold target [7,8]. For these collisions, bremsstrahlung radiation is mainly measured in the vicinity of the short–wavelength limit (SWL), where the electron transfers all its kinetic energy to the photon. The SWL is of particular interest since, due to the large momentum transfer to the nucleus, close collisions between electron and nucleus are required. In this collision regime the relativistic effects and, hence, the polarization correlations become of paramount importance [9]. Therefore, experiments performed in the short–wavelength limit provide a stringent test of the relativistic theory of the bremsstrahlung process. To exploit the power of these experiments, further polarization studies are underway with high–energy beams (few MeV) of polarized electrons [3,4].

Theoretically, all radiation processes can be treated to first order in the coupling of the electron to the radiation field because of the smallness of the fine structure constant, $e^2/\hbar c = 1/137.04$. Nevertheless, an accurate description of bremsstrahlung in the high–Z domain

is not a simple task because it requires the use of relativistic Dirac wavefunctions both for the initial and final electronic states. Since both these states belong to the (positive–energy) Dirac continuum, their partial–wave expansion has to be employed for practical calculations. In the past, such partial–wave, fully relativistic calculations have been successfully employed to study the (differential) bremsstrahlung cross sections for collision energies ranging from a few keV to 10 MeV [10]–[14], including the ultrarelativistic limit [15]. Less theoretical data are available, however, for the *polarization properties* of bremsstrahlung radiation especially in the ultra–relativistic regime where the rigorous relativistic calculations are often hampered by the slow convergence of the partial–wave expansion. In order to provide reliable theoretical predictions for the bremsstrahlung radiation in the high– and ultra– relativistic regimes, alternative approaches are required which are less demanding from a computational point of view. In this contribution we propose the Dirac–Sommerfeld–Maue (DSM) theory in which the incoming electron is described by the Sommerfeld–Maue function [16], while the scattered electron is represented in terms of a Dirac wave. This theory was recently introduced in Ref. [17] with the main emphasis on the doubly–differential cross sections and its predictions have been compared with those of the Elwert–Haug theory [18]–[20] and available experimental data. The DSM approach is expected to be well justified in the ultra–relativistic region for which the SM function is known to perform well [21,22]. To elucidate its validity we provide results for the polarization correlations both within the DSM and the partial–wave theory. By performing such a test, we concentrate on the SWL where these correlations are most pronounced.

The layout of the paper is the following. In Section 2 we provide the basic formulae for the polarization correlations and discuss how they can be parameterized in terms of the Stokes parameters. The evaluation of these parameters within the framework of the density matrix theory is discussed briefly in Section 2.2. In particular, we demonstrate how the analysis of the polarization properties of bremsstrahlung radiation can be traced back to the free–free transition amplitudes. The computation of these matrix elements, based on either the relativistic partial–wave theory or the DSM approach, is discussed in Sections 2.3 and 2.4, respectively. In section 3.1 the validity of the DSM model is tested numerically for electron scattering by bare silver (Ag^{47+}) and gold (Au^{79+}) ions and for a wide range of collision energies. Based on the results of this test, we employ in section 3.2 the DSM approach in order to analyze the polarization properties of the bremsstrahlung radiation in the high–relativistic regime. Finally, the conclusion is given in Section 4.

Atomic units ($\hbar = m = e = 1$) are used unless otherwise indicated.

2 Theory

Before we start discussing the polarization properties of bremsstrahlung radiation, let us first recall the basic notations and assumptions used throughout this paper. Since we restrict ourselves to the case of electron–nucleus (inelastic) scattering, the initial state of the overall system is given by a bare point–like nucleus with charge number Z and a free electron with total energy $E_i = \sqrt{k_i^2 c^2 + c^4} = T_{kin} + c^2$ and asymptotic momentum $\boldsymbol{k}_i$. The radiative, inelastic scattering of the electron leads to an emission of the photon with the wavevector $\boldsymbol{k}$ and polarization vector $\boldsymbol{e}_\lambda$. Moreover, in the short–wavelength limit the kinetic energy of the scattered electron is assumed to be *zero* and, hence, the bremsstrahlung photon has to carry away all the (initial) energy, $\omega = E_i - c^2$.

Besides the notation, we have to define the geometry in which the emission of bremsstrahlung photons is to be observed. In the present work, the polarization properties of the photons will be analyzed in the rest frame of the nucleus. Since in this frame the only preferred direction of the overall system is given by the initial electron momentum, we take the quantization axis (z–axis) along the direction of $\boldsymbol{k}_i$. Together with the wave vector of the bremsstrahlung photon, $\boldsymbol{k}$, this axis defines the reaction (x, z)-plane. Thus, only one polar angle θ_k is required to describe the photon emission. In contrast to the bremsstrahlung photon, the scattered electron is assumed to remain unobserved. The latter fact implies an integration of the triply differential bremsstrahlung cross section over the electron emission solid angle $d\Omega_f$ and a summation over its final spin states.

2.1 Polarization correlations and Stokes parameters

The polarization properties of bremsstrahlung radiation have been intensively studied over the past decades. In these studies, particular emphasis was laid on the question of how the spin states of the incident electrons affect the polarization of the bremsstrahlung photons. To explore such a "polarization transfer" phenomenon, the polarization correlations were introduced by Tseng and Pratt [9,23] who parameterized the bremsstrahlung differential cross section in terms of the spin polarization $\boldsymbol{n}_s$ of the impinging electron and a vector related to the photon polarization. For linearly polarized photons the polarization-dependent part of the cross section is determined by five parameters, from which only one is non–vanishing if the incoming electron beam is unpolarized (see Ref. [23] for further details).

While the polarization correlation parameters appear to be a very useful tool for the theoretical analysis of the bremsstrahlung process, it has been found more convenient for practical applications to describe the polarization properties of emitted photons in terms of Stokes parameters. These parameters are often utilized in experiments for characterizing the degree of polarization of the emitted light. Namely, the Stokes parameter P_3 reflects the degree of circular polarization and the two parameters P_1 and P_2 together denote the degree and direction of the linear polarization of the light. The latter two parameters are determined by measuring the intensitiy $I(\phi)$ of the light which is linearly polarized at different angles ϕ with

respect to the reaction (x,z)–plane [17,24,25]:

$$P_1 \;=\; \frac{I(0)-I(90^\circ)}{I(0)+I(90^\circ)}\,,\;\; P_2 \;=\; \frac{I(45^\circ)-I(135^\circ)}{I(45^\circ)+I(135^\circ)}\,. \quad (2.1)$$

These two parameters can be easily "visualized" if one represents the linear polarization of the bremsstrahlung radiation in terms of a polarization ellipse, defined in the plane perpendicular to the photon momentum $\boldsymbol{k}$. The principal axis of such an ellipse is characterized by its tilt angle χ with respect to the reaction plane [25],

$$\tan 2\chi \;=\; \frac{P_2}{P_1}\,, \quad (2.2)$$

and by its length $P_L = \sqrt{P_1^2+P_2^2}$ that reflects the *degree* of linear polarization. By making use of new Compton polarimeters the degree P_L and the tilt angle χ can be measured directly [7,8] such that the Stokes parameters P_1 and P_2 might be extracted from $P_1 = P_L\cos(2\chi)$ and $P_2 = P_L\sin(2\chi)$.

2.2 Density matrix approach

The theoretical analysis of the Stokes parameters (2.1) can be performed most efficiently within the framework of the density matrix approach [24,25]. Since during the last years this approach has been widely applied to the analysis of the polarization properties of the radiative recombination photons, we will restrict ourselves to a short compilation of the basic formulae relevant for our analysis and refer for all further details to the literature [26,25].

The density matrix approach is based on the fact that the experimentally measured photon polarization is a statistical average over the polarization directions of the individual photons emitted during the collision of an electron beam with the target. Consequently, the spin (polarization) state of such an ensemble can not be described by a single state vector (or wavefunction) but rather in terms of the spin–density matrix. Since for the photon there exist only two polarization states, one can use the same formalism as for spin–$\frac{1}{2}$ particles and define a 2×2 matrix which can be parameterized by the three (real) Stokes parameters:

$$\left(\langle \boldsymbol{k}\boldsymbol{e}_\lambda\,|\hat{\varrho}_\gamma|\,\boldsymbol{k}\boldsymbol{e}_{\lambda'}\rangle\right)_{\lambda,\lambda'=\pm1} = \frac{I}{2}\begin{pmatrix} 1+P_3 & P_1-iP_2 \\ P_1+iP_2 & 1-P_3 \end{pmatrix}, \quad (2.3)$$

where I is the total intensity of the radiation (e.g. $I = I(0)+I(90^\circ)$). Here we make use of the so–called *helicity* representation of the density matrix with $\lambda = \pm1$ being the photon helicity (i.e., the spin projection onto the direction of propagation). The basis vectors $\boldsymbol{e}_{+1}$ and $\boldsymbol{e}_{-1}$ are usually associated with the right– and left–circular polarization, respectively. These vectors can be written in terms of the *linear* polarization vectors $\boldsymbol{e}_x$, $\boldsymbol{e}_y$, defined in the plane that is perpendicular to the photon momentum $\boldsymbol{k}$ and lying *in* ($\boldsymbol{e}_x$) and *perpendicular* ($\boldsymbol{e}_y$) to the reaction plane, as $\boldsymbol{e}_{+1} = \frac{1}{\sqrt{2}}(\boldsymbol{e}_x + i\boldsymbol{e}_y)$ and $\boldsymbol{e}_{-1} = \frac{1}{\sqrt{2}}(\boldsymbol{e}_x - i\boldsymbol{e}_y)$. By using this relation between the circular $\boldsymbol{e}_{\pm1}$ and the linear $\boldsymbol{e}_{x,y}$ polarization vectors we follow the convention introduced by Rose in Ref. [27]. Note that such a convention implies signs for the parameters P_1 and P_2 in Eq. (2.3) opposite to those from Ref. [24].

As seen from Eq. (2.3), the Stokes parameters can be expressed in terms of the elements of the spin–density matrix. For the electron–nucleus bremsstrahlung, these matrix elements are obtained by standard techniques:

$$\langle \boldsymbol{k}\boldsymbol{e}_\lambda\,|\hat{\varrho}_\gamma|\,\boldsymbol{k}\boldsymbol{e}_{\lambda'}\rangle = N_0 \sum_{\sigma_f}\sum_{\sigma_i\sigma_i'} \left(\boldsymbol{e}_\lambda^*\boldsymbol{W}_{rad}(\sigma_i,\sigma_f)\right) \times \left(\boldsymbol{e}_{\lambda'}^*\boldsymbol{W}_{rad}(\sigma_i',\sigma_f)\right)^* \langle\sigma_i\,|\hat{\varrho}_i|\,\sigma_i'\rangle\,, \quad (2.4)$$

where the initial–state density matrix elements $\langle\sigma_i\,|\hat{\varrho}_i|\,\sigma_i'\rangle$ describe the polarization state of the incoming electron beam, and the transition amplitudes are given by

$$\boldsymbol{e}_\lambda^*\boldsymbol{W}_{rad}(\sigma_i,\sigma_f) \;=\; \int d\boldsymbol{r}\; \psi_{\boldsymbol{k}_f}^{(\sigma_f)\dagger}(\boldsymbol{r})\;(\boldsymbol{\alpha}\boldsymbol{e}_\lambda^*)\;\psi_{\boldsymbol{k}_i}^{(\sigma_i)}(\boldsymbol{r})\;e^{-i\boldsymbol{k}\boldsymbol{r}}\,. \quad (2.5)$$

Here $\psi_{\boldsymbol{k}_i}$ and $\psi_{\boldsymbol{k}_f}$ describe the initial and final electron with spin projection σ_i and σ_f, respectively, and $\boldsymbol{\alpha}$ is the vector of Dirac matrices. The normalization constant N_0 in (2.4) does not enter into the Stokes parameters P_k since they are defined by cross section *ratios*, cf. (2.1) and (2.3).

2.3 Evaluation of the radiation matrix element in the partial–wave–decomposition approach

As seen from Eqs. (2.3)–(2.5) any further analysis of the polarization properties of bremsstrahlung radiation can be traced back to the transition amplitudes $\boldsymbol{e}_\lambda^*\boldsymbol{W}_{rad}(\sigma_i,\sigma_f)$. In general, the evaluation of these matrix elements is not a simple task since they involve continuum solutions for both the initial and the final electronic states. However, within the short–wavelength limit, where the electron in its final state has *zero* kinetic energy, $\boldsymbol{e}_\lambda^*\boldsymbol{W}_{rad}(\sigma_i,\sigma_f)$ can be obtained by extrapolating the *free–bound* transition amplitudes to the continuum threshold of the Dirac spectrum [28,29]. During the last two decades the fully relativistic form of the bound–free transition matrix has been widely used for studying the radiative recombination of high–Z ions at intermediate and high collision energies [25,26,30,31]. For a capture into bare ions, it reads

$$\boldsymbol{e}_\lambda^*\boldsymbol{W}_{rad}{}^{\rm b}(\sigma_i) \;=\; \int d\boldsymbol{r}\; \psi_{n_f l_f j_f \mu_f}^{\dagger}(\boldsymbol{r})\;(\boldsymbol{\alpha}\boldsymbol{e}_\lambda^*)\;\psi_{\boldsymbol{k}_i}^{(\sigma_i)}(\boldsymbol{r})\;e^{-i\boldsymbol{k}\boldsymbol{r}}\,, \quad (2.6)$$

where $\psi_{n_f l_f j_f \mu_f}(\boldsymbol{r})$ and $\psi_{\boldsymbol{k}_i}^{(\sigma_i)}(\boldsymbol{r})$ are the known solutions of the Dirac Hamiltonian for a bound and continuum electron, respectively. For a point–like nucleus model, Eq. (2.6) can be computed analytically by using the calculus of the irreducible tensor operators and the hypergeometric functions. This usually requires the decomposition of both the photon as well as the continuum wavefunctions into partial multipole waves [14,23,32]. Since these calculations

are well–established nowadays, we will not recall them here and refer for all further details to the literature [30, 33–35].

As seen from Eq. (2.6), the bound–free transition amplitude describes the electron recombination into a bound state $|n_f l_f j_f \mu_f\rangle$ with well–defined total angular momentum j_f, its projection μ_f and parity $(-1)^{l_f}$ where l_f is the angular momentum of the large components of the Dirac spinor. However, no particular symmetry or parity can be attributed to the outgoing (continuum) electron following the bremsstrahlung process. Therefore, in order to employ the radiative recombination amplitudes for the description of bremsstrahlung at the short–wavelength limit, one has to sum in Eq.(2.6) over the final subshells $(l_f j_f \mu_f)$, when passing to the limit $n_f \to \infty$. Since in our "scenario" the scattered, final–state electron remains unobserved in the bremsstrahlung process, these bound–state subshells (respectively the continuum–state multipoles) have to be added *incoherently* and, hence, no information is required on their relative phases.

Several numerical tests have been performed by us to verify the application of Eq. (2.6), in the limit $n_f \to \infty$, for the accurate description of the polarization properties of bremsstrahlung radiation at the short–wavelength limit [36]. It was found that even though rather high values of the principal quantum number, $n_f \approx 15 - 20$, have to be used, the summation over the subshells $(l_f j_f \mu_f)$ can be restricted to just a few terms. For such a choice of computational parameters, good agreement (on the level of 0.5%) between "true" bremsstrahlung calculations and radiative–recombination–extrapolation results was found for collisions of electrons with high–Z bare ions for a wide range of (initial) energies, 50 keV $\leq T_{kin} \leq$ 3 MeV. By performing calculations at the high–energy edge of this interval we were faced with the well-known problem of the slow convergence of the partial–wave expansion. That is, owing to numerical problems in handling the rapid oscillations of the (high–energy) incident electron wavefunction, only a limited number of partial waves can be taken into account in the decomposition of $\psi^{(\sigma_i)}_{\boldsymbol{k}_i}(\boldsymbol{r})$ in Eq. (2.6). Such a truncation leads to a loss of accuracy of the partial–wave calculations for large energies of the incoming electron and backward photon emission angles.

2.4 Evaluation of the radiation matrix element in the DSM model

Since the DSM approach is discussed in detail in our previous work [17] we restrict ourselves here to a collection of the basic formulae. The fast incoming electron is described by a Sommerfeld–Maue function [18,22] which reads, when spherical coordinates (r, ϑ, φ) are used,

$$\psi^{(\sigma_i)}_{\boldsymbol{k}_i}(\boldsymbol{r}) = N_{k_i}\, e^{ik_i r\cos\vartheta}\{{}_1F_1(i\eta_i, 1, ik_i r(1-\cos\vartheta)) + \frac{iZ}{2c}\,[\alpha_z(\cos\vartheta - 1) + \frac{1}{2}\alpha_- \sin\vartheta\, e^{i\varphi} + \frac{1}{2}\,\alpha_+ \sin\vartheta\, e^{-i\varphi}] \times {}_1F_1(1 + i\eta_i, 2, ik_i r(1-\cos\vartheta))\}\, u^{(\sigma_i)}_{k_i}\,, \tag{2.7}$$

where $\eta_i = ZE_i/k_i c^2$, $\alpha_\pm = \alpha_x \pm i\alpha_y$, and the normalization constant is given by $N_{k_i} = (2\pi)^{-\frac{3}{2}} e^{\pi\eta_i/2}\Gamma(1 - i\eta_i)$. Moreover, in Eq. (2.7), ${}_1F_1$ is a confluent hypergeometric function and $u^{(\sigma_i)}_{k_i}$ denotes the (free) electron four–spinor. For an electron being polarized along its direction of propagation $\boldsymbol{k}_i$, i.e. $\boldsymbol{n}_s = (0, 0, 1)$ which we refer to as longitudinal polarization, this spinor is given by $u^{(\sigma_i)}_{k_i} = u^{(+)}_{k_i}$, where

$$u^{(+)}_{k_i} \;=\; C_{k_i} \begin{pmatrix} 1 \\ 0 \\ ck_i/(E_i + c^2) \\ 0 \end{pmatrix}, \quad C_{k_i} \;=\; \left(\frac{E_i + c^2}{2E_i}\right)^{\frac{1}{2}}. \tag{2.8}$$

For an arbitrary direction of $\boldsymbol{n}_s$ the electron spinor can always be re–written in terms of any two linearly independent basis elements $u^{(+)}_{k_i}$ and $u^{(-)}_{k_i} = C_{k_i}\,(0, 1, 0, -ck_i/(E_i + c^2))^t$.

In contrast to the approximate initial electronic function (2.7), we describe the (slow) outgoing electron by the exact relativistic Dirac function using the partial–wave representation. In the short-wavelength limit where the momentum of the scattered electron $k_f \to 0$, the large and small radial components of the partial waves can be expressed in terms of Bessel functions J_ν [11,37],

$$\begin{aligned} f_{jl}(r) &= \frac{1}{r}\,\frac{\kappa}{|\kappa|}\,\frac{1}{c}\,\sqrt{\frac{Z}{k_f}}\; J_{2\gamma_f}(\sqrt{8Zr})\,, \\ g_{jl}(r) &= -\,\frac{1}{r}\,\frac{\kappa}{|\kappa|}\,\frac{1}{\sqrt{k_f Z}}\,\Big[\sqrt{2Zr}\; J_{2\gamma_f - 1}(\sqrt{8Zr}) \\ &\quad -\;\; (\gamma_f + \kappa)\; J_{2\gamma_f}(\sqrt{8Zr})\Big]\,, \end{aligned} \tag{2.9}$$

where

$$\gamma_f \;=\; \sqrt{\kappa^2 - (Z/c)^2}, \qquad \kappa \;=\; \begin{cases} -(l+1), & j = l + \frac{1}{2} \\ \;\;\; l, & j = l - \frac{1}{2} \end{cases}. \tag{2.10}$$

Both, Sommerfeld–Maue and Dirac continuum–electron wavefunctions from above are normalized according to $\int \psi^{(\sigma_f)\,*}_{\boldsymbol{k}_f}(\boldsymbol{r})\, \psi^{(\sigma_f)}_{\boldsymbol{k}'_f}(\boldsymbol{r})\, d\boldsymbol{r} = \delta(\boldsymbol{k}_f - \boldsymbol{k}'_f)$.

By inserting the initial– and the final–state electron wavefunctions into Eq. (2.5) the transition matrix element $\boldsymbol{e}^*_\lambda \boldsymbol{W}_{rad}$ can be reduced to a sum of two–dimensional integrals (over r and ϑ) which are evaluated numerically with the help of convergence generating functions, $e^{-\epsilon r}$, with ϵ being small enough such that stability is obtained. For the SWL only a few (typically 3-5) partial waves are needed to describe the slow outgoing electron when the collision energy is high [38]. The relative error of the DSM calculations (concerning the step numbers in the double integral as well as the choice of the exponential cutoff factor in the radial integral) is below 5 % in the forward hemisphere but maybe reach up to 10 % for the backward emission angles (for P_2 at the largest E_i). Further inaccuracies, which result from truncating the final–state partial–wave series beyond $j = \frac{3}{2}$, occur at small angles, but have decreased well below 5 percent when $T_{kin} \geq 2$ MeV.

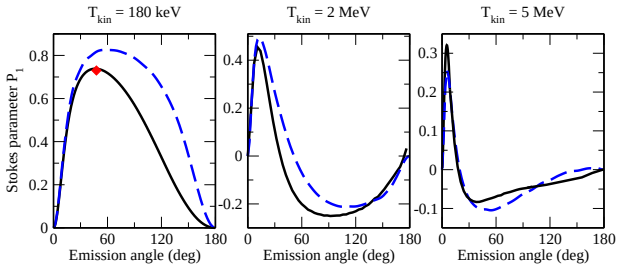

Fig. 1. The Stokes parameter P_1 of the bremsstrahlung radiation emitted in collisions of unpolarized electrons with bare gold ions. Results are presented for the Dirac–Sommerfeld–Maue approach (dashed line) as well as for the partial–wave–decomposition theory (solid line) for three collision energies T_{kin} = 180 keV, 2 MeV and 5 MeV. In the left panel, the theoretical prediction by Brysk and co–workers [11] is displayed in addition by a solid diamond.

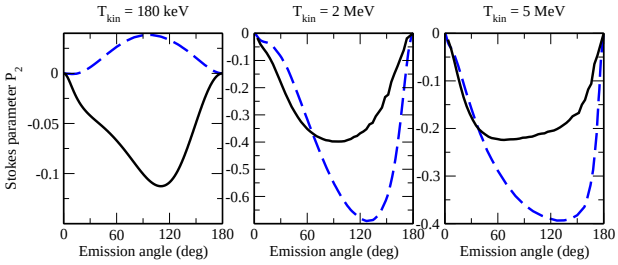

Fig. 2. The Stokes parameter P_2 of the bremsstrahlung radiation emitted in collisions of longitudinally polarized electrons with bare gold ions. Results are presented for the Dirac–Sommerfeld–Maue approach (dashed line) as well as for the partial–wave–decomposition theory (solid line) for three collision energies T_{kin} = 180 keV, 2 MeV and 5 MeV.

3 Results and discussion

3.1 Accuracy test of the DSM approach

In order to investigate the validity of the Dirac–Sommerfeld–Maue method and to explore the limits of its applicability detailed calculations have been performed for the linear polarization of the bremsstrahlung photons emitted in energetic collisions of electron beams with medium– and high–Z bare ions. In these calculations special attention has been paid to the short–wavelength limit where DSM results have been compared with the predictions of the Dirac partial–wave theory discussed in Section 2.3. In Fig. 1 we display the Stokes parameter P_1 obtained for electron scattering by a gold (Au^{79+}) target as a function of photon emission angle θ_k for collision energies in the range 180 keV $\leq T_{kin} \leq$ 5 MeV. The left panel of the figure also shows the result by Brysk and co–workers [11] who performed partial–wave calculations by using threshold continuum states for the emitted electron. For the single emission angle, $\theta_k = 47.7°$, for which results were reported in Ref. [11], there is a very good agreement with the present partial–wave results. Moreover, these results describe an experimental data point for P_1 at 180 keV [39] also very well.

Turning to the comparison between the theoretical models, it is seen from the left panel of Fig. 1 that for the relatively low collision energy of 180 keV the Dirac–Sommerfeld–Maue theory fails to reproduce the polarization parameter P_1 for emission angles $\theta_k > 20°$. The large discrepancy between the predictions of the DSM approach and the partial–wave relativistic theory observed at this weak–relativistic impact energy ($\gamma_i = 1/\sqrt{1-(v/c)^2} \approx 1.35$), confirms that—for such low energies—the Sommerfeld–Maue function (2.7) is inappropriate for the description of the electron motion in the Coulomb field of heavy nuclei [40]. When the energy is increased to 2 MeV, as shown in the middle panel, the discrepancies between the Dirac–Sommerfeld–Maue model and the partial–wave theory have considerably diminished, even though the DSM calculations still overestimate the linear polarization of the emitted photons in the forward hemisphere. Finally, for 5 MeV, the DSM results are converging to the exact ones except for large angles (cf. right panel of Fig.1). These large angles, however, are not of interest for future bremsstrahlung experiments since—for high collision energies $\gtrsim$ 5 MeV — emission of the bremstrahlung radiation occurs predominantly in the forward directions, $\theta \lesssim 10°$.

Until now we have analyzed the polarization parameter P_1 which is known to be *non–zero* even for collisions of unpolarized electrons with (unpolarized) ions. In order to discuss the effect of polarization transfer we turn now to the second Stokes parameter P_2 which can be used for the diagnostics of electron beam polarization. Owing to its spin–dependence, this parameter appears to be a more sensitive probe of relativistic effects. This can be seen from Fig. 2 where we display P_2 calculated for collisions of longitudinally polarized electrons with bare gold ions. Obviously, the qualitative agreement between the DSM model and the relativistic partial–wave theory, established for P_1 when $T_{kin} \approx$ 2 MeV, does no longer hold for P_2 at such an impact energy. Only for $T_{kin} \approx$ 5 MeV and for the forward emission angles, the DSM approach provides reasonable predictions for the second Stokes parameter P_2 (cf. right panel of Fig. 2).

Besides the gold target, detailed polarization calculations have also been performed for the (radiative) electron scattering by medium–Z ions. Fig. 3 displays, for example, the parameters P_1 and P_2 of the bremsstrahlung radiation emitted in collisions of longitudinally polarized electrons with bare silver (Ag^{47+}). For this—lighter—target and for collision energies 2 MeV and 5 MeV, the DSM model performs better than for the $Z = 79$ case (compare with Figs. 1–2). We can understand such a Z–behaviour of the DSM predictions if we recall the criterion of validity of the Sommerfeld–Maue function at high energies, $r \gtrsim Z/k_i c$, where r is the electron–nucleus distance [22]. This criterion implies that for lower charges Z the accuracy of the SM function improves for small r thus allowing for more precise calculations of the Stokes parameters.

In order to better understand the incident–polarization dependence of P_2, we investigated this parameter also for

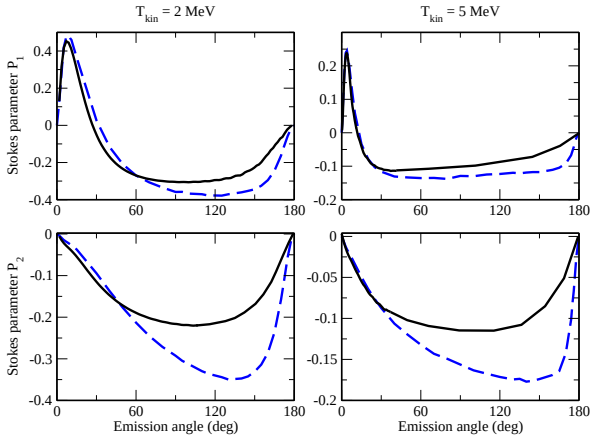

Fig. 3. The Stokes parameters P_1 and P_2 of the bremsstrahlung radiation emitted in collisions of longitudinally polarized electrons with bare silver ions. Results are presented for the Dirac–Sommerfeld–Maue approach (dashed line) as well as for the partial–wave–decomposition theory (solid line) for the collision energies T_{kin} = 2 MeV and 5 MeV.

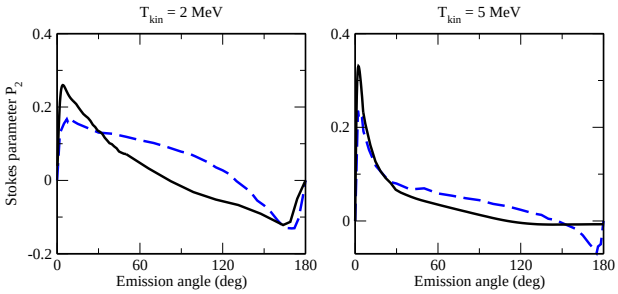

Fig. 4. The Stokes parameter P_2 of the bremsstrahlung radiation emitted in collisions of transversely polarized electrons with bare silver ions. Results are presented for the Dirac–Sommerfeld–Maue approach (dashed line) as well as for the partial–wave–decomposition theory (solid line) for the collision energies T_{kin} = 2 MeV and 5 MeV.

the transverse spin polarization (along the x–axis) of the incoming electrons. Such a geometry can be experimentally verified with the help of a Wien filter [41]. The results for Ag^{47+}, displayed in Fig. 4, indicate that in the forward hemisphere the agreement between the DSM model and the rigorous relativistic theory is worse than for the case of the longitudinal polarization. For $T_{\rm kin}$ = 2 MeV both rigorous relativistic and DSM approaches predict that P_2 acquires positive values reaching a maximum near $\theta_k = 5°$. The Dirac–Sommerfeld–Maue calculations considerably underestimate, however, the maximum value of the polarization. Only for higher energies, $T_{\rm kin} \gtrsim 5$ MeV, the performance of the DSM model improves so that it allows to describe reasonably well the second Stokes parameter in the experimentally relevant region of small emission angles $\theta_k \lesssim 30°$.

3.2 Properties of polarization correlations in the high–relativistic regime

As seen from the results presented in Figures 1-4, the Dirac–Sommerfeld–Maue approach provides a reasonable estimate of the linear polarization of bremsstrahlung photons emitted in forward directions and for collision energies near and above 5 MeV, the more so, the lighter the target. Therefore, in such a high–relativistic regime, the DSM approximation can be employed instead of the (standard) partial–wave–expansion techniques which may suffer from convergence problems if the incoming electron velocity becomes too high. The combination of these two models thus allows for the calculation of the polarization correlations in a very wide parameter range.

In order to illustrate the application of the DSM theory to the analysis of the bremsstrahlung radiation in the high–relativistic regime and to better understand the energy–dependence of the linear polarization, detailed calculations of the Stokes parameters have been performed for collision energies up to 15 MeV. Even though the theory can be employed even for higher energies, this would require an accurate treatment of the nuclear–size effects which is out of the scope of this paper. In Fig. 5 we display the second Stokes parameter P_2 of the bremsstrahlung radiation following inelastic scattering of longitudinally polarized electrons by bare gold ions. Calculations have been performed for the energy range $2 \le T_{kin} \le 15$ MeV and within two approximations. While for the (comparatively) low energies T_{kin} = 2 and 5 MeV we used the relativistic partial–wave theory, theoretical predictions for 15 MeV have been obtained in the DSM approach. As seen from the figure, the absolute value of P_2 strongly decreases with collision energy in a wide angular range. A similar behaviour is found for the second Stokes parameter calculated for *transversely* polarized (incoming) electrons. For this case the maximum value of the (degree of) polarization, which is reached at 5 MeV (see also Fig. 4), drops to about half of it when the collision energy is further increased to 15 MeV (cf. Fig. 6).

4 Conclusion

In conclusion, the polarization correlations in the electron–nucleus bremsstrahlung have been explored under the assumption that the scattered, final–state electron remains unobserved. In our study special emphasis was placed on the experimentally relevant regime of high–Z targets and collision energies in the range from 180 keV to 15 MeV. For these energies, detailed calculations were performed within the short-wavelength limit (SWL) for the linear polarization of the bremsstrahlung photons and for various polarization states of the incident electron beam. The polarization correlations were explored by means of a rigorous relativistic theory and the hybrid Dirac–Sommerfeld–Maue approach that employs the Dirac solution only for the description of the (slow) scattered electron. By comparing predictions of these two theories for the various

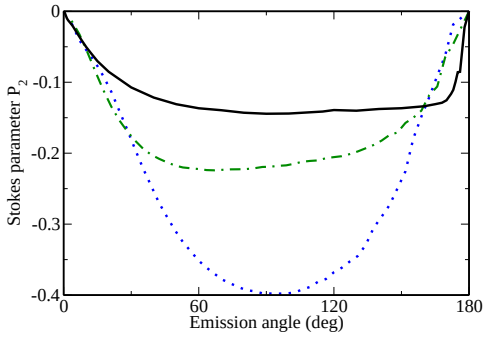

Fig. 5. The Stokes parameter P_2 of the bremsstrahlung radiation emitted in collisions of longitudinally polarized electrons with bare gold ions. Calculations have been performed for collision energies: 2 MeV (dotted line, partial–wave results), 5 MeV (dash–dotted line, partial–wave results) and 15 MeV (solid line, DSM results).

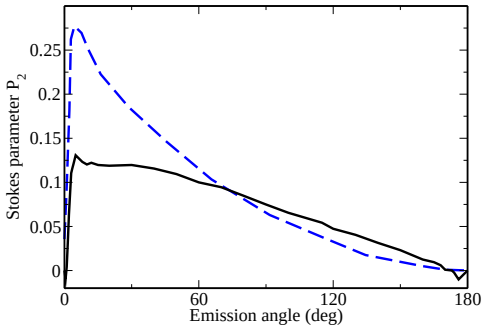

Fig. 6. The Stokes parameter P_2 of the bremsstrahlung radiation emitted in collisions of transversally polarized electrons with bare gold ions. Calculations have been performed for two collision energies: 5 MeV (dashed line, partial–wave calculations) and 15 MeV (solid line, DSM calculations).

polarization correlation parameters, we were able to show that the DSM model provides a *complementary* approach to the partial–wave theory in the high–relativistic regime.

The comparison between DSM and partial–wave predictions also gives more insight into the behaviour of the Sommerfeld–Maue wavefunction. For example, the Stokes parameter P_1 of the emitted radiation, which is nonzero even in the non–relativistic limit and which generally decreases with collision energy (eventually to negative values) reflects the behaviour of the wavefunction well away from the nucleus. When approximate, DSM data for this parameter are compared to exact partial–wave results, it is concluded that globally the SM function performs well at energies above 2 MeV. In contrast, P_2 provides a tool for testing the innermost spatial region of the electronic function, especially at large photon angles. There, the discrepancies between DSM and exact relativistic calculations are most prominent, due to the missing relativistic contraction of the SM function. We recall that at very small distances the Sommerfeld–Maue function gets only exact in the limiting case $\gamma_i \to \infty$. One can expect, therefore, that in such an ultra–relativistic limit, the Dirac–Sommerfeld–Maue theory will be appropriate for an accurate description of the P_2 parameter in the whole angular range.

Based on the calculations presented in Section 3 we estimate the range of validity of the Dirac–Sommerfeld–Maue approach (for high Z and $\gamma_i \gg 1$) to be given roughly by $Z/(\gamma_i v) \approx Zc/E_i \lesssim 0.02$. Within this parameter range and for the forward emission angles, the DSM model provides an accurate estimate for both Stokes parameters P_1 and P_2. Since for relativistic electrons with energies $E_i > 2$ MeV the photons are predominantly emitted into a narrow cone around the incoming beam axis ($\theta_k = 0°$), this model may be used to analyze the outcome of future high–energy bremsstrahlung experiments. Such experiments are planned to be performed in the nearest future at the Facility for Antiproton and Ion Research (FAIR) as well as at the Technical University of Darmstadt and are expected to reveal unique information about the fundamental process of electron–photon interaction in the ultra–relativistic regime.

Acknowledgments

A.S. acknowledges support from the Helmholtz Gemeinschaft (Nachwuchsgruppe VH–NG–421).

References

1. S.Tashenov et al, Phys. Rev. Lett. **97**, 223202 (2006)
2. U.Spillmann et al, Rev. Sci. Instrum. **79**, 083101 (2008)
3. R.Barday et al, WSPC Proceedings (2009), and PESP Proceedings (2010)
4. F.Nillius and K.Aulenbacher, PESP Proceedings (2010)
5. O.Klein, Y.Nishina, Z. Physik **52**, 853 (1929)
6. G. Weber et al, Phys. Rev. Lett. **105**, 243002 (2010)
7. S.Tashenov et al, submitted for publication
8. R.Märtin et al, Contributed paper to CAARI, Denton, Texas (2010)
9. H.K.Tseng, R.H.Pratt, Phys. Rev. A**7**, 1502 (1973)
10. J.D.Rozics, W.R.Johnson, Phys. Rev **135**, B56 (1964)
11. H.Brysk, C.D.Zerby, S.K.Penny, Phys. Rev. **180**, 104 (1969)
12. H.K.Tseng, R.H.Pratt, Phys. Rev. A**3**, 100 (1971)
13. H.K.Tseng, R.H.Pratt, Phys. Rev. A **19**, 1525 (1979)
14. E.Haug, Eur. Phys. J. D **58**, 297 (2010)
15. R.J.Jabbur, R.H.Pratt, Phys. Rev. **133**, B1090 (1964)
16. A.Sommerfeld, A.W.Maue, Ann. Physik **22**, 629 (1935)
17. D.H.Jakubassa-Amundsen, Phys. Rev. A **82**, 042714 (2010)
18. H.Olsen, L.C.Maximon, Phys. Rev. **114**, 887 (1959)
19. G.Elwert, E.Haug, Phys. Rev. **183**, 90 (1969)
20. E.Haug, Phys. Rev. **188**, 63 (1969)
21. H. A. Bethe, L. C. Maximon, Phys. Rev. **93**, 768 (1954)

22. V.B.Berestetskii, E.M.Lifshitz, L.P.Pitaevskii, *Quantum Electrodynamics* Vol. 4 of Course of Theoretical Physics (Elsevier, Oxford, 1982) §39
23. H.K.Tseng, J. Phys. B **35**, 1129 (2002)
24. K.Blum, *Density Matrix Theory and Applications* (Plenum Press, New York, 1996) Second Edition, Sections 1.2, 3.3, 3.5
25. A.Surzhykov, S.Fritzsche, Th.Stöhlker, S.Tashenov, Phys. Rev. A**68**, 022710 (2003)
26. A.Surzhykov, S.Fritzsche, Th.Stöhlker, Phys. Lett. A**289**, 213 (2001)
27. E.M.Rose, *Elementary theory of angular momentum* (John Wiley, New York, 1957) §28.
28. C.M.Lee, R.H.Pratt, Phys. Rev. A **12**, 1825 (1975)
29. I.J.Feng, I.B.Goldberg, Young Soon Kim, R.H.Pratt, Phys. Rev. A **28**, 609 (1983)
30. J.Eichler, Th.Stöhlker, Phys. Rep. **439**, 1 (2007)
31. A.Surzhykov, S.Fritzsche, Th.Stöhlker, S.Tashenov, Phys. Rev. Lett. **94**, 203202 (2005)
32. I.Øverbø, K.J.Mork, H.A.Olsen, Phys. Rev. A **8**, 668 (1973)
33. S.R.Valluri, U.Becker, N.Grün, W.Scheid, J. Phys. B: At. Mol. Opt. Phys. **17**, 4359 (1984)
34. J.Eichler, W.Meyerhof, *Relativistic atomic collisions* (Academic Press, San Diego, 1995)
35. A.Surzhykov, S.Fritzsche, Th.Stöhlker, J. Phys. B: At. Mol. Opt. Phys. **35**, 3713 (2002)
36. V.Yerokhin, A.Surzhykov, Phys. Rev. A **82**, 062702 (2010)
37. V.S.Popov, Sov. J. Nucl. Phys. **12**, 235 (1971)
38. R.H.Pratt, H.K.Tseng, Phys. Rev. A **11**, 1797 (1975)
39. M.Scheer, E.Trott, G.Zahs, Z. Phys. **209**, 68 (1968)
40. J.K.Fink, R.H.Pratt, Phys. Rev. A **7**, 392 (1973)
41. M.Salomaa, H.A.Enge, Nucl. Instr. Meth. **145**, 279 (1977)